Atomic-dipole squeezing and emission spectra of the nondegenerate two-photon Jaynes-Cummings model

M. M. Ashraf and M. S. K. Razmi*
Department of Physics, Quaid-I-Azam University, Islamabad, Pakistan
(Received 19 August 1991)

A nondegenerate two-photon Jaynes-Cummings model is analyzed for its atomic-dipole squeezing and emission spectra. The input fields are assumed to be coherent or squeezed. The atomic dipole squeezes both for the on- and off-resonance excitations, showing a greater amount of squeezing for the former. The emission spectrum shows a central-two-peak structure for a variety of field inputs. When the fields are initially in coherent or squeezed states, sidebands appear whose widths are governed by the input-field statistics.

PACS number(s): 42.52.+x, 42.50.Dv

I. INTRODUCTION

With the successful operation [1] in a high-Q cavity of a single-mode two-photon maser, the discussions of the nondegenerate two-photon Jaynes-Cummings model (NTPJCM) have acquired added importance. Although previous attempts [2] to obtain lasing through two-mode two-photon-mediated transitions have met with only limited success, the advent of additional techniques [3] of demonstrating cavity QED effects has considerably brightened up the prospects of achieving this goal. A number of dynamical aspects of the NTPJCM, including field squeezing [4], have been studied recently [5]. We believe that these studies should be complemented by a discussion of a number of other important issues, such as atomic-dipole squeezing and the emission spectra. We address these problems in the present paper.

It is by now well known that in a squeezed state of the field one obtains reduced fluctuations in one quadrature at the expense of increased fluctuations in the other. In much the same way as for the field annihilation operator, one can decompose the atomic-dipole operator into its dispersive and absorptive parts and investigate whether any of them display a reduced noise that is mandated by an atomic analogy of the zero-point field fluctuations. It is known, for example, that the one-photon JCM [6] exhibits both field squeezing [7] and atomic dipole squeezing [8]. Similarly, both types of squeezing are seen to arise [9,10] in the interaction of a three-level atom with a coherent field. As we show later, the NTPJCM also exhibits atomic-dipole squeezing for a variety of field inputs.

The nature of the interaction of an atom with the cavity field will profoundly influence the characteristics of light emitted from it. This realization has prompted several studies [11–15] of the emission spectrum of a cavity-bound atom and has led to the discovery of a number of nonclassical phenomena, including vacuum-field Rabi splitting [12]. The framework for computation of such spectra has been laid by Eberly and co-workers [11,12,16], and we follow their procedure in computing the results for the NTPJCM.

The paper is organized as follows. We introduce atomic-dipole squeezing in Sec. II and work out the relevant quantities using the NTPJCM. Numerical results are presented and discussed in Sec. III. The emission spectrum is calculated in Sec. IV where its numerical analysis and discussion are also carried out.

II. ATOMIC-DIPOLE SQUEEZING IN THE NTPJCM

A two-level atom is most conveniently described by the Pauli lowering and raising operators σ and $\sigma^\dagger$ and the inversion operator $\sigma_3=\sigma^\dagger\sigma-\sigma\sigma^\dagger$. The dispersive and absorptive components of the slowly varying dipole operators may be written [11] as

$$\sigma_1=\tfrac{1}{2}(\sigma^\dagger e^{-i\omega_0 t}+\sigma e^{i\omega_0 t}) , \tag{1}$$

and

$$\sigma_2=\frac{1}{2i}(\sigma^\dagger e^{-i\omega_0 t}-\sigma e^{i\omega_0 t}) , \tag{2}$$

respectively. The commutation relation

$$[\sigma_1,\sigma_2]=(i/2)\sigma_3 \tag{3}$$

leads to the following Heisenberg uncertainty relation:

$$(\Delta\sigma_1)^2(\Delta\sigma_2)^2\geq\tfrac{1}{16}|\langle\sigma_3\rangle|^2 , \tag{4}$$

where

$$(\Delta\sigma_i)^2=\langle\sigma_i^2\rangle-\langle\sigma_i\rangle^2 , \quad i=1,2 .$$

The atomic state is said to be squeezed if

$$(\Delta\sigma_i)^2<\tfrac{1}{4}|\langle\sigma_3\rangle| , \quad i=1 \text{ or } 2 . \tag{5}$$

Since

$$(\Delta\sigma_l)^2=\tfrac{1}{4}-\begin{cases}(\mathrm{Re}\langle\sigma\rangle e^{i\omega_0 t})^2 , & l=1\\ (\mathrm{Im}\langle\sigma\rangle e^{i\omega_0 t})^2 , & l=2\end{cases} \tag{6}$$

the squeezing condition (5) can also be written

$$S_1 \equiv \frac{[1-4(\mathrm{Re}\langle\sigma\rangle e^{i\omega_0 t})^2]}{|\langle\sigma_3\rangle|} < 1$$

or

$$S_2 \equiv \frac{[1-4(\mathrm{Im}\langle\sigma\rangle e^{i\omega_0 t})^2]}{|\langle\sigma_3\rangle|} < 1 \ . \tag{7}$$

The NTPJCM Hamiltonian in the rotating-wave approximation is given by

$$H = \tfrac{1}{2}\hbar\omega_0\sigma_3 + \hbar(\omega_1 a_1^\dagger a_1 + \omega_2 a_2^\dagger a_2) + \hbar\lambda(a_1^\dagger a_2^\dagger \sigma + \text{c.c.}) \ . \tag{8}$$

Let $|+\rangle$ and $|-\rangle$ denote the excited and ground states of the atom. Assuming that at $t=0$ the atom is in the excited state and the two fields in mixtures of Fock states, the initial atom-field (AF) wave function can be written

$$|\psi_{\mathrm{AF}}(0)\rangle = \sum_{n_1,n_2} C_{n_2}^{(1)} C_{n_2}^{(2)} |+;n_1,n_2\rangle \ , \tag{9}$$

where $C_{n_i}^{(i)}$ are the number-state expansion coefficients $C_{n_i}^{(i)} = \langle n_i|\psi_{\mathrm{F}}(0)\rangle$. If the two fields are initially in the coherent state,

$$C_{n_i}^{(i)} = (n_i!)^{-1/2}(\bar{n}_i)^{n_i/2}\exp\left[-\frac{\bar{n}_i}{2}\right] , \tag{10}$$

and the initial mean photon number is given by $\bar{n}_i = |\alpha_i|^2$, where α_i are the coherent excitation parameters of the two fields. If, on the other hand, the two fields are in the squeezed state, we have [4]

$$C_{n_i}^{(i)} = (n_i!\mu_i)^{-1/2}(\nu_i/2\mu_i)^{n_i/2} H_{n_i}(\beta_i/\sqrt{2\mu_i\nu_i}) \times \exp\left[-\tfrac{1}{2}|\beta_i|^2 + \frac{\nu_i^*}{2u_i}\beta_i^2\right] , \tag{11}$$

$$\mu_i = \cosh r_i \ , \quad \nu_i = e^{i\vartheta_i}\sinh r_i \ , \quad \beta_i = \mu_i\alpha_i + \nu_i\alpha_i^* \ .$$

Here r_i are the squeeze parameters, ϑ_i the squeeze angles, and α_i the coherent excitation parameters. For simplicity of calculation, we set $\vartheta_i = 0$ and take α_i to be real from now on. The initial mean photon number is given by $\bar{n}_i = |\alpha_i|^2 + \sinh^2 r_i$.

Proceeding in the standard fashion we find that

$$\langle\sigma\rangle e^{i\omega_0 t} = \sum_{n_1,n_2} \rho_{n_1+1,n_1}^{(1)} \rho_{n_2+1,n_2}^{(2)} A_{n_1+1,n_2+1}(t) \times B_{n_1+1,n_2+1}^*(t) \ , \tag{12}$$

$$\langle\sigma_3\rangle = \sum_{n_1,n_2} \rho_{n_1 n_1}^{(1)} \rho_{n_2 n_2}^{(2)} [\,|A_{n_1 n_2}(t)|^2 - |B_{n_1+1,n_2+1}(t)|^2] \ , \tag{13}$$

where

$$A_{n_1 n_2}(t) = e^{-i\phi t}\left[\cos\Omega t - i\frac{\Delta}{2\Omega}\sin\Omega t\right] ,$$

$$B_{n_1+1,n_2+1}(t) = -i(\lambda/\Omega)\sqrt{(n_1+1)(n_2+1)}\,e^{-i\phi t}\sin\Omega t \ ,$$

$$\phi = \phi_{n_1 n_2} = (n_1+\tfrac{1}{2})\omega_1 + (n_2+\tfrac{1}{2})\omega_2 \ , \tag{14}$$

$$\Omega = \Omega_{n_1 n_2} = \left[\frac{\Delta^2}{4} + \lambda^2(n_1+1)(n_2+1)\right]^{1/2} ,$$

$$\Delta = \omega_0 - \omega_1 - \omega_2 \ .$$

Note that $\rho_{nn'} = C_n C_{n'}^*$.

III. RESULTS AND DISCUSSION

The results for the squeezing functions S_1 and S_2 for different input parameters in the case of on-resonance excitations ($\Delta = 0$) are shown in Figs. 1–4. Both in the case of moderate ($\bar{n}_1 = 15$, $\bar{n}_2 = 10$) and high ($\bar{n}_1 = 60$, $\bar{n}_2 = 50$) input intensities, we find that the dispersive component does not squeeze at all whether the input fields are both squeezed or coherent. S_2, on the other hand, goes below the standard quantum limit with virtually no time delay, and recurrently. When the field intensities are relatively moderate and the inputs are coherent, S_2 shows squeezing only for the initial moments of the atom-field interaction ($\lambda t \le 0.05$) after which squeezing is revoked permanently. With higher coherent-input intensities S_2 still shows squeezing during the interval $0 < \lambda t \le 0.05$, though, unlike the preceding case, it suffers repeated desqueezing as well during this short span of time. That is, the net duration of squeezing grows smaller. Interestingly, however, the degree of squeezing grows larger in going from moderate to high intensities. The cases with squeezed inputs (Figs. 2 and 4) also share these features. The degree as well as the duration of squeezing here are, however, larger than those found in the case of coherent inputs. For the sake of completeness, we should mention here that squeezing does not show up in either case until after $\bar{n}_i \ge 7.0$, and even then the degree of squeezing is

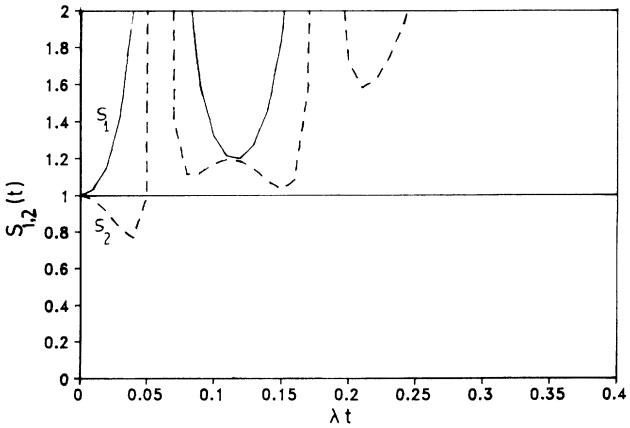

FIG. 1. The squeezing functions S_1 and S_2 for a coherent-field input with $\bar{n}_1 = 15$, $\bar{n}_2 = 10$, and $\Delta = 0$.

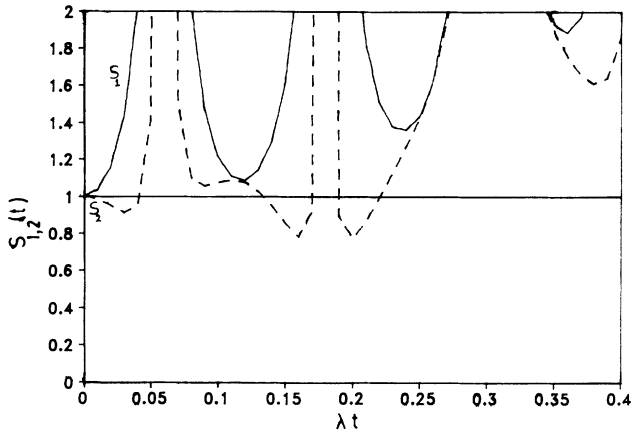

FIG. 2. S_1 and S_2 for a squeezed-field input with $\bar{n}_1=15$, $\bar{n}_1=10$, $r_1=1.0$, $r_2=0.8$, and $\Delta=0$.

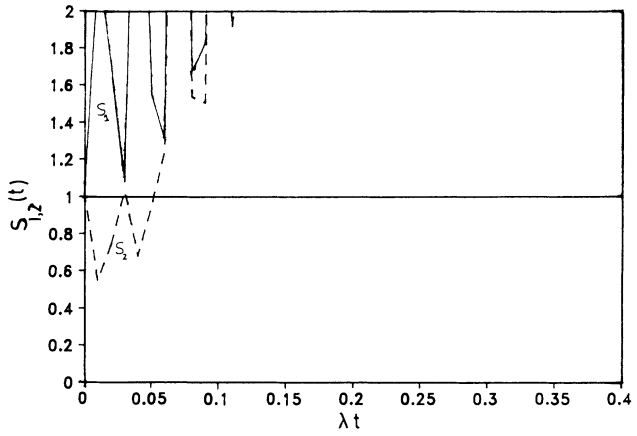

FIG. 3. S_1 and S_2 for a coherent-field input with $\bar{n}_1=60$, $\bar{n}_2=50$, and $\Delta=0$.

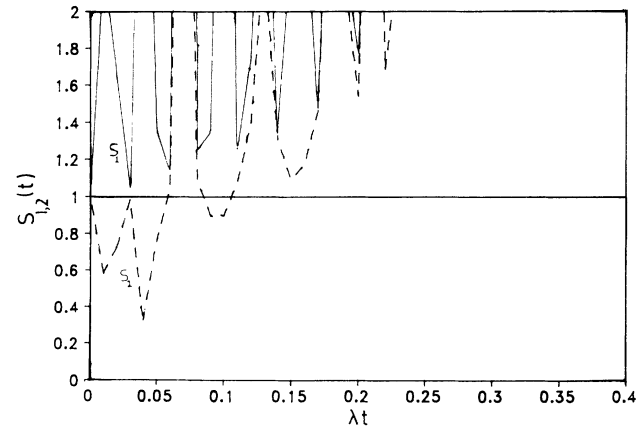

FIG. 4. S_1 and S_2 for a squeezed-field input with $\bar{n}_1=60$, $\bar{n}_2=50$, $r_1=1.0$, $r_2=0.8$, and $\Delta=0$.

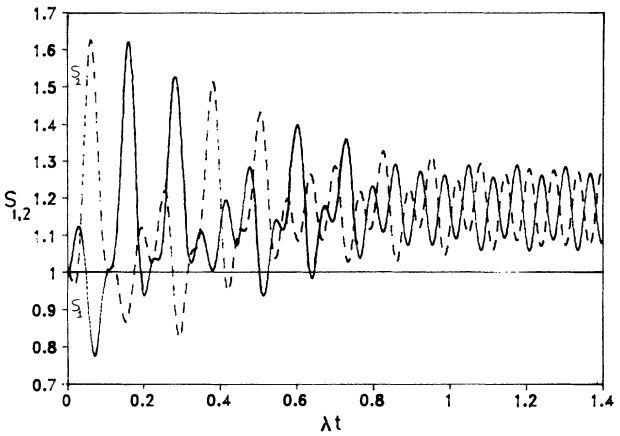

FIG. 5. S_1 and S_2 for a coherent-field input with $\bar{n}_1=15$, $\bar{n}_2=10$, and $\Delta=-50$.

small enough to be negligible.

The time evolution for S_1 and S_2 for the case of off-resonance excitations ($\Delta\neq 0$) is shown in Figs. 5–8. Unlike the on-resonance case, both S_1 and S_2 squeeze recurrently (the desqueezing of S_1 in Fig. 7 is due to large input intensities). The difference in the statistical properties of the input fields is reflected in the duration and degree of squeezing. Thus, with a squeezed-field input, the maximum squeezing achieved in Fig. 6 is approximately 12%, which occurs in S_2, but for coherent inputs of the same intensities (Fig. 5) it is 22% occurring in S_1. Similarly, for $\bar{n}_1=60$, $\bar{n}_2=50$, the maximum squeezing achieved is approximately 40% in S_1 with squeezed inputs (Fig. 8) and 38% in S_2 with coherent inputs (Fig. 7). In this case too, the values of $\bar{n}_1$ and $\bar{n}_2$ must exceed a certain threshold (≥ 7.0) to be able to yield noticeable squeezing. In any case, with the increase in $\bar{n}_i$ the maximum value of squeezing increases and its occurrence is hastened.

A comparison of the two excitation types (on-resonance and off-resonance) with the same $\bar{n}_i$ shows that

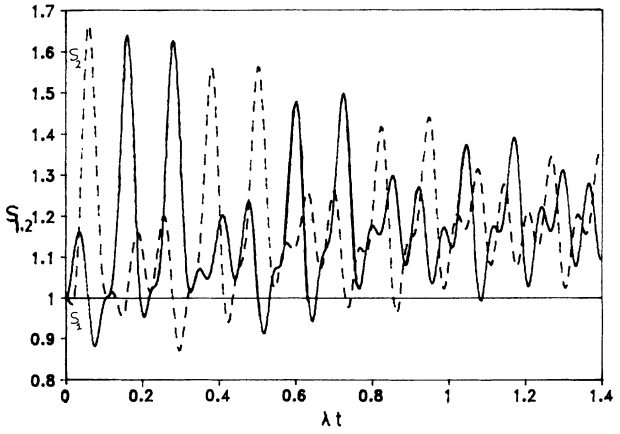

FIG. 6. S_1 and S_2 for a squeezed-field input with $\bar{n}_1=15$, $\bar{n}_2=10$, $r_1=1.0$, $r_2=0.8$, and $\Delta=-50$.

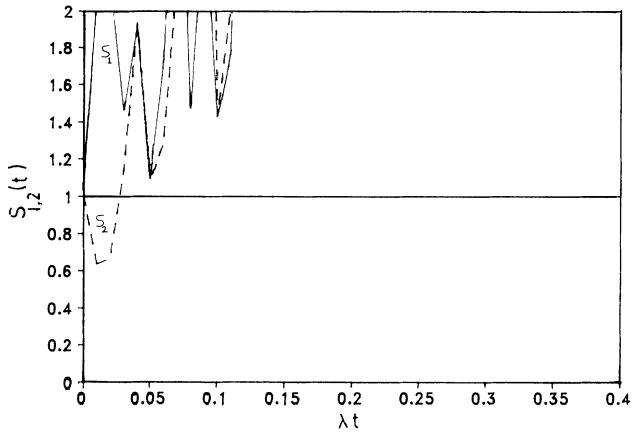

FIG. 7. S_1 and S_2 for a coherent-field input with $\bar{n}_1=60$, $\bar{n}_2=50$, and $\Delta=-50$.

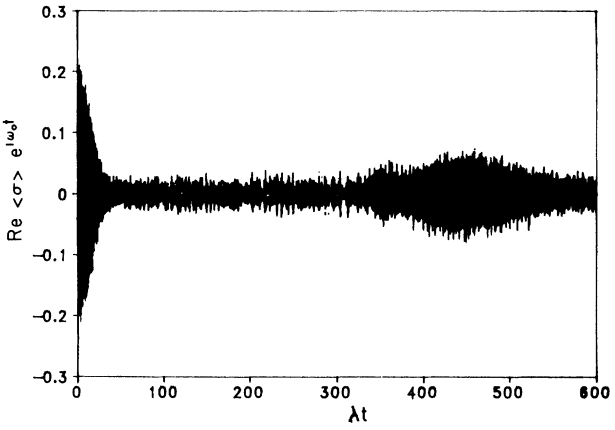

FIG. 9. The dispersive component $\mathrm{Re}\langle\sigma\rangle e^{i\omega_0 t}$ for a coherent-field input with $\bar{n}_1=15$, $\bar{n}_2=10$, $\Delta=-50$.

the $\Delta=0$ excitations lead to greater amounts of squeezing when initially both fields are either coherent or squeezed. However, the reduced dipole fluctuations last longer in the $\Delta\neq 0$ case. It is also instructive to note that the population inversion $\langle\sigma_3\rangle$ collapses to a zero value when $\Delta=0$ and to a nonzero value when $\Delta\neq 0$. This explains the large values achieved by the squeezing functions in the on-resonance case.

An inspection of the inequalities (7) reveals that for squeezing to exist both $\langle\sigma_3\rangle$ and $\langle\sigma\rangle$ must assume large values. We show the time evolution for $\mathrm{Re}\langle\sigma\rangle e^{i\omega_0 t}$ in Figs. 9 and 10 for the coherent and squeezed inputs, respectively. In either case, this quantity shows a closely spaced succession of collapses and revivals (which, however, are relatively better resolved in the case of squeezed input). The oscillations start damping out right after the interaction is turned on, and even in the first major revival (seen after $\lambda t>400$) the amplitudes do not equal the initial amplitudes. We also computed the time evolution of population inversion corresponding to the initial conditions of Figs. 9 and 10. As expected, we encounter collapses and revivals of the Rabi oscillations. The first collapse is followed by a period of quiescence after which revivals wand collapses take place in such rapid succession that no complete collapse occurs after the first one. However, for $t>0$, the envelope of the Rabi oscillations fails to build up beyond a point where its amplitude is only a fraction of the initial amplitudes. Viewing together the behavior of $\langle\sigma\rangle$ and $\langle\sigma_3\rangle$ we discover why the onset of atomic-dipole squeezing and its revocation happens so soon (in less than time λ^{-1}) after turning on the atom-field interaction.

It is useful to compare these results with those of the single-photon Jaynes Cummings model. For the latter case, the time evolution of $\mathrm{Re}\langle\sigma\rangle e^{i\omega_0 t}$ with a coherent input is shown in Fig. 11. The Rabi envelope consists of a fairly wide strip with angular excursions placed regularly on both sides. The full width of the strip is roughly equal to the largest amplitude of oscillation. The envelope never collapses to zero. In the NTPJCM case, however, the Rabi envelope comes very close to showing a total collapse, especially with a squeezed input. Thus

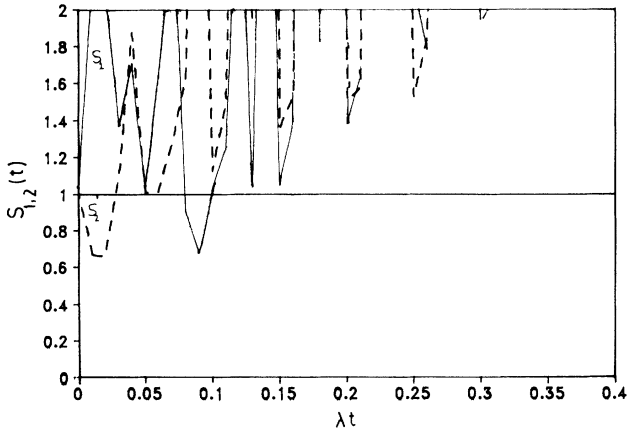

FIG. 8. S_1 and S_2 for a squeezed-field input with $\bar{n}_1=60$, $\bar{n}_2=50$, $r_1=1.0$, $r_2=0.8$, and $\Delta=-50$.

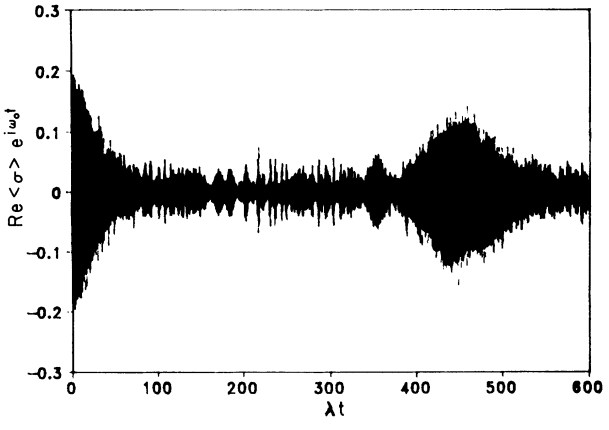

FIG. 10. $\mathrm{Re}\langle\sigma\rangle e^{i\omega_0 t}$ for a squeezed-field input with $\bar{n}_1=15$, $\bar{n}_2=10$, $r_1=1.0$, $r_2=0.8$, and $\Delta=-50$.

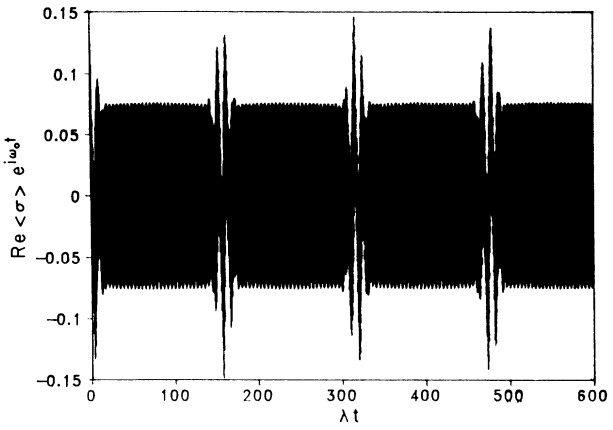

FIG. 11. $\mathrm{Re}\langle\sigma\rangle e^{i\omega_0 t}$ for a coherent-field input $\bar{n}=15$, $\Delta=-50$, for a one-photon JCM.

squeezing is more likely to occur for a longer period of time in the one-photon JCM. This is borne out by a recently published calculation [8].

Finally, we note that the time interval during which the population inversion remains clamped at a constant value is marked by rapid oscillations of the dipole moment. This implies that the relative phase between the pair of states (from excited to virtual and from virtual to ground) shifts with time without affecting, however, the dynamical equilibrium of the atomic transitions.

A number of authors have attempted to see relationships between atomic and field squeezing. For example, Walls and Zoller [17] have pointed out the existence of a simple relationship between two types of squeezing in resonance fluorescence. Similarly, Wodkiewicz *et al* [18] have shown that, under certain conditions, a relationship exists in the case of superposition states of the field. In the case of NTPJCM, the corresponding relationship is quite complex and we do not stop to reproduce it here. The lack of the existence of a simple relationship can be seen directly by comparing our curves of atomic-dipole squeezing with those of Gou [5] of field squeezing.

IV. EMISSION SPECTRUM

The physical transient spectrum is given by the expression [16]

$$S(\nu)=2\Gamma\int_0^T dt_1\int_0^T dt_2\exp[-(\Gamma-i\nu)(T-t_1) -(\Gamma+i\nu)(T-t_2)] \times\langle\psi_{\mathrm{AF}}|\sigma^\dagger(t_1)\sigma(t_2)|\psi_{\mathrm{AF}}\rangle\ , \quad (15)$$

where T is the time at which the measurement takes place and Γ^{-1} is the response time of the filter. Since we wish to compute the emission spectrum, $|\psi_{\mathrm{AF}}\rangle$ in (15) is given by Eq. (9).

In the Heisenberg picture, the dipole operator evolves according to the relation

$$\sigma(t)=U^\dagger(t)\sigma(0)U(t)\ ,\quad U(t)=e^{-(i/\hbar)Ht}\ . \quad (16)$$

To compute the action of $\sigma(t)$ on the state $|+;n_1,n_2\rangle$, it is best to diagonalize H in the manifold of bare states $|+;n_1,n_2\rangle$ and $|-;n_1+1,n_2+1\rangle$. Proceeding in this manner, we find that

$$\sigma(t)|+;n_1,n_2\rangle =f_{n_1n_2}(t)[g_{n_1-1,n_2-1}(t)|+;n_1-1,n_2-1\rangle +f_{n_1-1,n_2-1}(t)|-;n_1,n_2\rangle]e^{-i(\omega_0-\Delta)t}\ , \quad (17)$$

where

$$f_{n_1n_2}(t)=\tfrac{1}{2}\left[\left[1+\frac{\Delta}{2\Omega}\right]e^{-i\Omega t}+\left[1-\frac{\Delta}{2\Omega}\right]e^{i\Omega t}\right]\ ,$$
$$g_{n_1n_2}(t)=\tfrac{1}{2}\left[\left[1-\frac{\Delta^2}{4\Omega^2}\right]^{1/2}\left[e^{i\Omega t}-e^{-i\Omega t}\right]\right]\ . \quad (18)$$

We obtain, therefore, the result that

$$\langle\psi_{\mathrm{AF}}|\sigma^\dagger(t_1)\sigma(t_2)|\psi_{\mathrm{AF}}\rangle =e^{-i(\omega_0-\Delta)(t_2-t_1)}\sum_{n_1,n_2}\rho^{(1)}_{n_1n_1}\rho^{(2)}_{n_2n_2}f^*_{n_1n_2}(t_1)f_{n_1n_2}(t_2) \times f_{n_1-1,n_2-1}(t_2-t_1)\ . \quad (19)$$

Substituting (19) in (15) and carrying out the indicated integration we get an expression for the emission spectrum:

$$S(\nu)=\sum_{n_1,n_2}\rho^{(1)}_{n_1n_1}\rho^{(2)}_{n_2n_2}S_{n_1n_2}(\nu)\ , \quad (20)$$

with

$$S_{n_1n_2}(\nu)=\frac{\Gamma}{4}[|F^+_{n_1n_2}(\Omega,\Omega')+F^+_{n_1n_2}(-\Omega,\Omega')|^2 +|F^+_{n_1n_2}(-\Omega,-\Omega')+F^+_{n_1n_2}(\Omega,-\Omega')|^2] \quad (21)$$

and

$$F^+_{n_1n_2}(\Omega,\Omega') =\left[1+\frac{\Delta}{2\Omega}\right]\left[1+\frac{\Delta}{2\Omega'}\right]^{1/2} \times\frac{\exp[i(\omega_0-\nu+\Omega+\Omega'-\Delta)T]-\exp(-\Gamma T)}{\Gamma+i(\omega_0-\nu+\Omega+\Omega'-\Delta)}\ . \quad (22)$$

Note that Ω is given in (14) and Ω' is obtained from it by the replacements $n_1\rightarrow n_1-1$, $n_2\rightarrow n_2-1$.

Equation (20) gives the emission spectrum as a sum over spectra of the pure number states of the fields appropriately weighted with their photon number distributions. We look, therefore, at the behavior of $S_{n_1n_2}(\nu)$ for some particular values of n_1 and n_2.

Because of the four sign combinations in (21) one expects to see four peaks; in general they occur at

$\omega_0-\nu=\Delta\pm(\Omega+\Omega')$ and $\omega_0-\nu=\Delta\pm(\Omega-\Omega')$. However, for $\Delta=0$, $\Omega'=\lambda\sqrt{n_1 n_2}$ so that Ω' vanishes when either n_1 or n_2 vanishes. We then obtain only two peaks located at $\pm\Omega=\pm\lambda\sqrt{(n_1+1)(n_2+1)}$, as shown in Fig. 12. When $n_1=n_2=0$, the peak locations are $\pm\lambda$. This is the vacuum field Rabi splitting [12]. When $n_1=0$ and $n_2\neq 0$, the peaks are located at $\pm\lambda\sqrt{n_2+1}$, and move away from each other with increasing n_2. In any case, we get a two-peak structure when one of the fields is in the vacuum state and the other in a number state. In some sense this seems counterintuitive when a comparison is made with the one-photon JCM [13]. In the latter case, one gets a four-peak structure for a number state $|n\rangle$, $n\geq 1$. When n increases, the inner two peaks coalesce and the outer ones recede away from each other, leading to a three-peak structure.

Now consider the case when $\Delta=0$ and n_1 and n_2 re nonzero. When $n_1=n_2$, the inner two peaks are always separated by the distance 2λ. When $n_1\neq n_2$, this distance may change. Barring extremely disparate values of n_1 and n_2, however, the separation between the inner peaks remains small enough to be visible in our graphs (see Fig. 13). In all cases, the outer peaks move away from each other when we increase n_1 and n_2. In this case, therefore, the four peaks will be seen only if n_1 and n_2 are not too large.

Let us now turn to the nonresonant case ($\Delta\neq 0$). When both files are in the vacuum state, the inner two peaks are located at

$$\omega_0-\nu=\Delta\pm\left[\left[\frac{\Delta^2}{4}+\lambda^2\right]^{1/2}-\frac{\Delta}{2}\right]$$

and the outer ones at

$$\omega_0-\nu=\Delta\pm\left[\left[\frac{\Delta^2}{4}+\lambda^2\right]^{1/2}+\frac{\Delta}{2}\right].$$

That is, both pairs are symmetrically situated about the point $\omega_0-\nu=\Delta$. If $\Delta\gg\lambda$, the inner two peaks occur at $\omega_0-\nu=\Delta\pm(\lambda^2/\Delta)$, i.e., the vacuum field Rabi splitting becomes much less transparent compared to the resonant case. Essentially the same situation exists when $n_1=0$, $n_2\neq 0$, but that $\Delta\gg\lambda n_2$. The central two-peak structure stands out clearly when the initial photon numbers are large enough to mask the effect of detuning $\lambda n_i\gg\Delta$. These peaks now occurs at

$$\omega_0-\nu=\Delta\pm\lambda[\sqrt{(n_1+1)(n_2+1)}-\sqrt{n_1 n_2}]\,.$$

Let us now discuss the case when one of the fields is in the vacuum state and the other in the *squeezed* vacuum state, shown in the Fig. 14. For the latter, ρ_{nn} is peaked

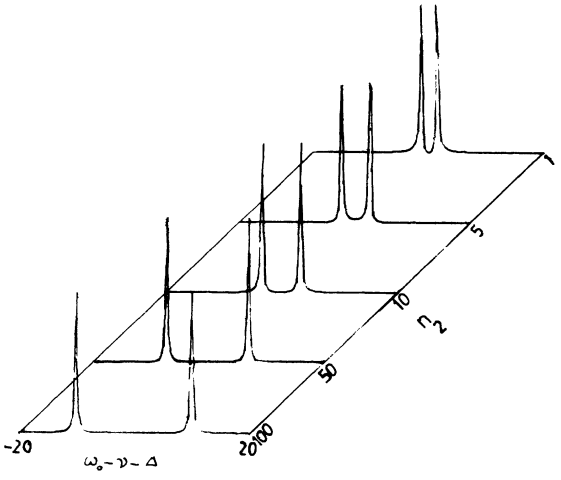

FIG. 12. The number-state spectra $S_{n_1 n_2}(\nu)$ for $n_1=0$, $\Delta=0$.

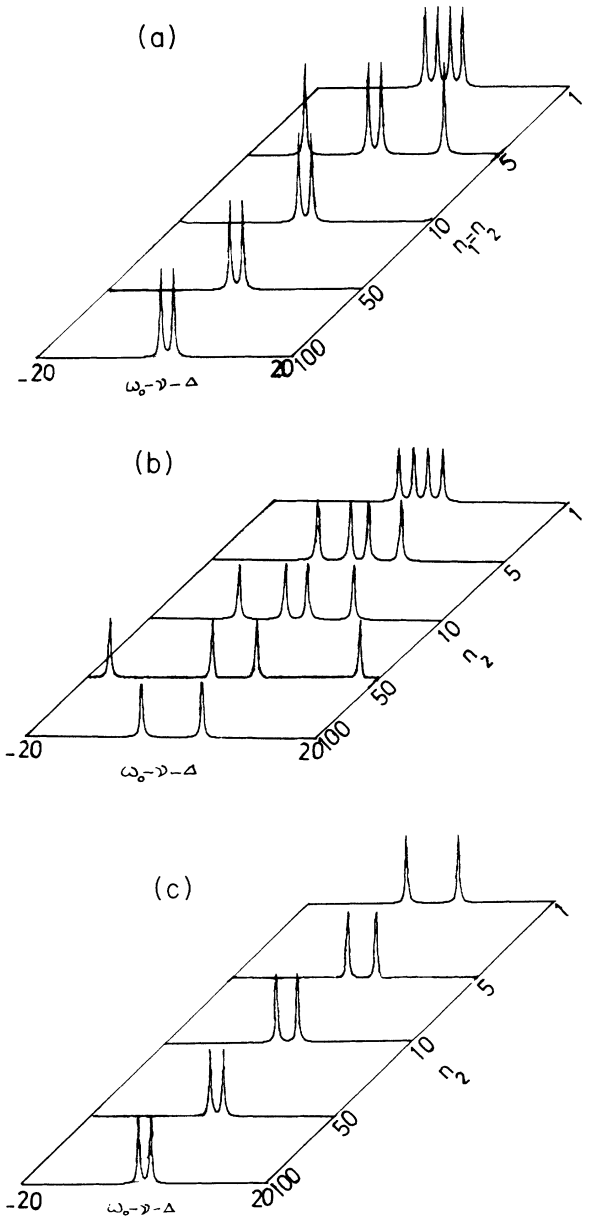

FIG. 13. $S_{n_1 n_2}(\nu)$ for (a) $n_1=n_2$; (b) $n_1=1$; (c) $n_1=100$. $\Delta=0$ in each case.

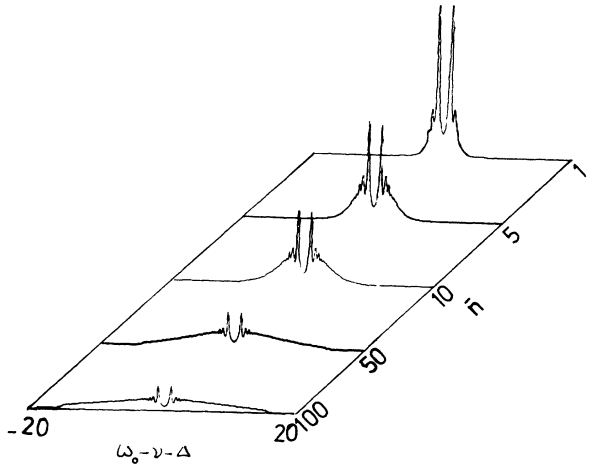

FIG. 14. The emission spectrum $S(\nu)$ when one field is in the vacuum state and the other in the *squeezed* vacuum state, with $\Delta=0$.

at $n=0$ and falls off sharply as we move away from this value. Also, $\rho_{nn}=0$ for odd values of n. The photon-number variance $(\Delta n)^2$ is proportional to $\bar{n}(\bar{n}+1)$, where $\bar{n}$ is the average photon number of the field. Referring to Eq. (20), it is clear that for small values of $\bar{n}$ the spectrum will be completely dominated by the Rabi peaks. As we increase $\bar{n}$, more and more of the photon-number-state spectra have to be included in the sum. However, because their weights keep decreasing, the central two-peak structure is only modified in the wings by the addition of smaller peaks. When the squeezed-vacuum field is replaced by a thermal field we get more or less the same results, a few minor differences notwithstanding.

We next turn to the case when one field is in the vacuum state and the other in a coherent state, shown in Fig. 15. Now, the photon distribution ρ_{nn} for a coherent state field is peaked at $\bar{n}$, with a width Δn of the order of $\sqrt{\bar{n}}$. The two-peak Rabi structure will show up as long as $\bar{n}$ is small. The values of n that contribute significantly to the sum on the right-hand side of (20) lie in range $\bar{n}-\sqrt{\bar{n}}$ to

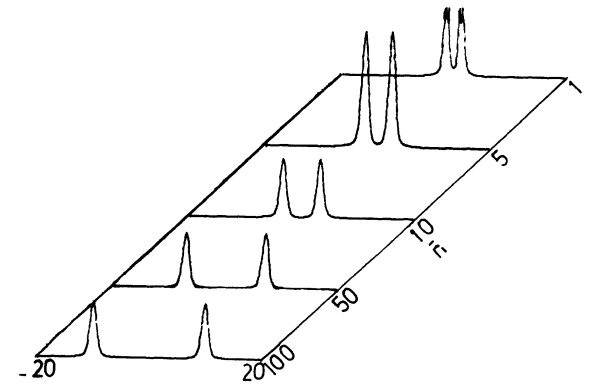

FIG. 15. $S(\nu)$ when one field is in the vacuum state and the other in a coherent state, with $\Delta=0$.

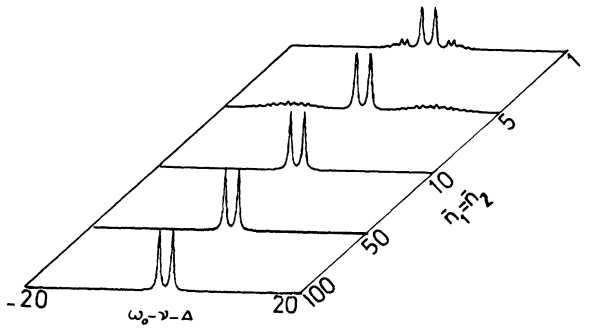

FIG. 16. $S(\nu)$ for both fields in squeezed vacuum, with $\Delta=0$.

$\bar{n}+\sqrt{\bar{n}}$. When $\bar{n}$ is large, the contributions of small-n values will be rendered less important; the Rabi peak structure will all but disappear and sidebands will appear of width λ (independent of $\bar{n}$), approximately centered at $\omega_0-\nu=\pm\lambda\sqrt{\bar{n}}$.

The foregoing discussion should be helpful in visualizing the emission spectrum when both fields have nonzero average photon numbers. Let us see the nature of this spectrum when the two fields are in squeezed-vacuum states. It is clear that as long as $\bar{n}_1$ and $\bar{n}_2$ are small, we should see only the Rabi peaks. As $\bar{n}_i$ increase, additional peaks have to be taken into account. However, because the multiplicative factors ρ_{nn} decrease rapidly with increasing n, the corresponding peak heights are severely limited. That is, on both sides of the central structure a series of small peaks should appear. This is confirmed by the spectra of Fig. 16.

We now consider the case of coherent inputs. When the initial photon numbers are small the spectrum is still dominated by the Rabi peaks. When $\bar{n}_i$ increase additional peaks appear on both sides of the central structure. Though the vacuum-field Rabi splitting is missing where large $\bar{n}_i$ are involved (a property peculiar to the Poissonian photon statistics, as explained earlier), the (large) n values lying in the range $(\bar{n}_i-\sqrt{\bar{n}_i})$ to $(\bar{n}_i+\sqrt{\bar{n}_i})$ by themselves produce a central-two-peak structure with a

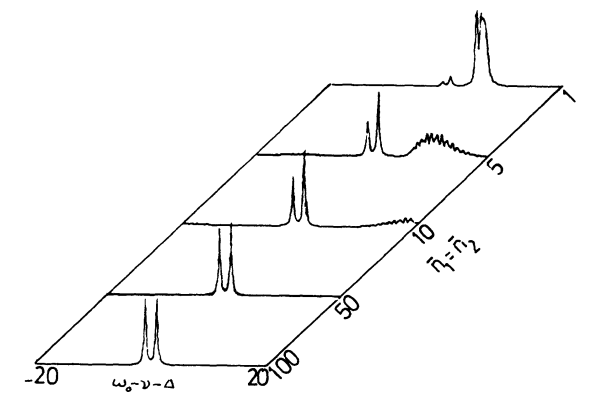

FIG. 17. $S(\nu)$ for both fields in coherent state, with $\Delta=5\lambda$.

separation of approximately 2λ. These peaks occur at the location $\omega_0-\nu=\pm(\Omega-\Omega')\simeq\pm\lambda$. Of course, there exist also sidebands of width $\lambda\sqrt{\bar{n}}$ that are too broad to be seen. Figure 17 displays the features mentioned above.

When the input files are squeezed, we get similar results to the coherent-input case. However, the widths of the sidebands could expand or shrink depending on whether we are dealing with super-Poissonian or sub-Poissonian fields.

ACKNOWLEDGMENT

This research was supported by a grant from the Pakistan Science Foundation.

*Deceased.

[1] M. Brune, J. M. Raimond, P. Goy, L. DAvidovich, and S. Haroche, Phys. Rev. Lett. **59**, 1899 (1987).

[2] J. Y. Goa, W. W. Eidson, M. Squicciarini, and L. M. Narduci, J. Opt. Soc. Am B **1**, 606 (1984).

[3] P. Goy, J. M. Raimond, M. Gross, and S. Haroche, Phys. Rev. Lett. **50**, 1903 (1983); D. Meschede, H. Walther, and G. Müller, *ibid.* **54**, 551 (1985); S. Haroche and J. M. Raimond, Adv. At. Mol. Phys. Rev. **20**, 239 (1985).

[4] H. P. Yuen, Phys. Rev. A **13**, 2226 (1976).

[5] Shih-Chaun Gou, Phys. Rev. A **40**, 5116 (1989); M. S. Abdalla, M. M. A. Ahmed, and A.-S. F. Obada, Physica A **162**, 251 (1990); **170**, 393 (1991).

[6] E. T. Jaynes and F. W. Cummings, Proc. IEEE **51**, 89 (1963).

[7] P. Meystre and M. S. Zubairy, Phys. Lett. **89A**, 390 (1982); A. S. Shumovsky, F. L. Kien, and E. I. Aliskenderov, Phys. Lett. A **124**, 351 (1987).

[8] X. S. Li, D. L. Lin, T. F. George, and Z. D. Liu, Phys. Rev. A **40**, 2504 (1989).

[9] X. S. Li, D. L. Lin, T. F. George, and Z. D. Liu, Phys. Rev. A **40**, 228 (1989).

[10] S. Y. Zhu, D. Liu, and X. S. Li, Phys. Lett. A **128**, 89 (1989).

[11] N. B. Narozhney, J. J. Sanchez-Mondragon, and J. H. Eberly, Phys. Rev. A **23**, 236 (1981).

[12] J. J. Sanchez-Mondragon, N. B. Narozhney, and J. H. Eberly, Phys. Rev. Lett. **51**, 550 (1983).

[13] J. Gea-Banacloche, R. R. Schlicher, and M. S. Zubairy, Phys. Rev. A **38**, 3514 (1988).

[14] V. Buzek and I. Jex, Quantum Opt. **2**, 147 (1990).

[15] V. Buzek, I. Jex, and M. Brisudova, Int. J. Mod. Phys. B **5**, 797 (1977).

[16] J. H. Eberly and K. Wodkiewicz, J. Opt. Soc. Am. **67**, 1252 (1977).

[17] D. F. Walls and P. Zoller, Phys. Rev. Lett. **47**, 709 (1981).

[18] K. Wodkiewicz, P. L. Knight, S. J. Buckle, and S. M. Barnett, Phys. Rev. A **35**, 2567 (1987).